Heliyon 10 (2024) e39006

Contents lists available at ScienceDirect

Heliyon

journal homepage: www.cell.com/heliyon

Research article

Characterizing metabolomic and transcriptomic changes, and investigating the therapeutic mechanism of *Psoralea corylifolia* linn. In the treatment of kidney-yang deficiency syndrome in rats

Ming-Liang Zhang [a,b,c], Wei-Xia Li [a,b,c,d], Xiao-Yan Wang [a,b,c], Xiao-Fei Chen [a,b,c], Hui Zhang [a,b,c], Gao-Quan Meng [d], Yu-Long Chen [d], Ya-Li Wu [a,b,c], Liu-Qing Yang [a,b,c], Shu-Qi Zhang [a,b,c], Ke-Ran Feng [a,b,c], Lu Niu [a,b,c], Jin-Fa Tang [a,b,c,d,*]

[a] *Department of Pharmacy, The First Affiliated Hospital of Henan University of Traditional Chinese Medicine, Zhengzhou, 450000, China*
[b] *Henan Province Engineering Research Center for Clinical Application, Evaluation and Transformation of Traditional Chinese Medicine, Zhengzhou, 450000, China*
[c] *Henan Provincial Key Laboratory for Clinical Pharmacy of Traditional Chinese Medicine, Zhengzhou, 450000, China*
[d] *Henan University of Traditional Chinese Medicine, Zhengzhou, China*

A R T I C L E I N F O

Keywords:
cAMP
Kidney-yang deficiency syndrome
Metabolomics
Psoralea corylifolia linn.
Transcriptomics

A B S T R A C T

Kidney-yang deficiency syndrome (KYDS) is characterized by a metabolic disorder stemming from neuroendocrine dysregulation, often associated with hepatic dysfunction. In traditional Chinese medicine, *Psoralea corylifolia* Linn. (BGZ) is commonly utilized for treating KYDS. However, the specific therapeutic effects of BGZ on liver function regulation remain unclear. To evaluate the protective effects of BGZ against KYDS in rats, organ index, alanine aminotransferase (ALT), aspartate aminotransferase (AST), and other biochemical indices were analyzed. Hematoxylin and eosin (HE) staining was utilized to assess liver histopathology. Additionally, transcriptomic and metabolomic analyses were conducted to identify potential biomarkers. BGZ treatment led to a significant reduction in ALT and AST levels, accompanied by improvements in liver histopathology in rats with KYDS. Moreover, BGZ induced significant alterations in 92 differentially expressed genes (DEGs) and 20 metabolites in the KYDS rat model. The comprehensive examination of metabolites and DEGs identified potential mechanisms underlying the therapeutic effects of BGZ, highlighting the neuroactive ligand-receptor interaction, cAMP signaling pathway, calcium signaling pathway, and cytokine-cytokine receptor interaction as key mechanisms. Validation of key targets within the cAMP pathway was substantiated through enzyme-linked immunosorbent assay and real-time quantitative polymerase chain reaction. The cAMP pathway emerges as a plausible mechanism through which BGZ exerts protective effects against KYDS. The findings of this study contribute to an improved understanding of the therapeutic actions of BGZ and establish a groundwork for further research into the complex pathways involved, as well as the potential for drug-targeted therapies for KYDS.

* Corresponding author. Department of Pharmacy, The First Affiliated Hospital of Henan University of Traditional Chinese Medicine, Zhengzhou, 450000, China.
E-mail address: a0519@163.com (J.-F. Tang).

https://doi.org/10.1016/j.heliyon.2024.e39006
Received 7 June 2024; Received in revised form 24 September 2024; Accepted 4 October 2024
Available online 5 October 2024

1. Introduction

Kidney-yang deficiency syndrome (KYDS) is a metabolic disorder with its conceptual origins in early Chinese medical literature [1], most notably in the "Yellow Emperor's Classic of Internal Medicine (Huangdi Neijing)" [2]. KYDS is characterized by neuroendocrine dysfunction, primarily involving multi-level dysregulation of the hypothalamus-pituitary-adrenocortical (HPA) axis, which affects the adrenal, thyroid, and gonadal systems. Clinically, KYDS presents with a range of symptoms including qi deficiency, cold extremities, limited mobility, delayed responsiveness, diminished appetite, aversion to cold, frequent urination, diarrhea, and hair thinning [3].

Recent research has underscored the close relationship between the neuroendocrine system and liver function, particularly regarding its role in emotional regulation [4]. Emotional fluctuations have been identified as potential triggers for cerebral cortex dysfunction, leading to disruptions in both the endocrine and immune systems [5]. Clinical investigations have demonstrated that KYDS is a common syndrome among chronic hepatitis B (HBV) carriers and individuals with dyslipidemia in traditional Chinese medicine (TCM) practice [6,7]. This observation suggests a potential direct correlation between abnormal liver function and KYDS. Consequently, the management of KYDS should incorporate careful monitoring of liver function.

Psoralea corylifolia Linn., known in TCM as Bu Gu Zhi (BGZ), has been extensively employed in Asian traditional medicine for centuries, attributed with a wide range of therapeutic effects. BGZ is particularly noted for its ability to enhance kidney function and reinforce yang, a concept in TCM associated with vital energy and metabolic processes. It is believed to consolidate essence, potentially addressing conditions associated with kidney deficiency, such as lumbar discomfort, frequent urination, infantile enuresis, and renal leakage. BGZ is also indicated for addressing warm spleen conditions—a TCM term for digestive imbalances characterized by symptoms like diarrhea—by mitigating diarrhea, facilitating Qi inhalation (vital energy intake), and alleviating asthma [8].

BGZ contains bioactive constituents, including psoralen, bakuchiol, psoralidin, and various flavonoids. These components confer BGZ with a range of pharmacological properties, such as anti-tumor, antioxidant, antibacterial, anti-inflammatory, antidepressant, estrogen regulation, bone growth promotion, and neuroprotection [9,10]. In TCM, BGZ is commonly employed for managing osteoporosis, with its principal active compounds psoralen and 5-methoxypsoralen, also being applied in the treatment of vitiligo and psoriasis [11,12]. While the therapeutic efficacy of BGZ in treating KYDS has been established through centuries of clinical practice in China, the precise mechanisms of its action remain unclear. This uncertainty poses a potential hazard to safe medication practices, as evidenced by recent case reports of liver injury associated with the use of BGZ and its compound preparations [13,14]. Therefore, a comprehensive understanding of the mechanism through which BGZ exerts its effects on KYDS is crucial for informing safe and effective clinical use.

KYDS induction in rats is commonly achieved through sustained intraperitoneal administration of high doses of exogenous glucocorticoids (GC), such as hydrocortisone, to create an animal model that replicates symptoms analogous to those observed in KYDS [15]. These models are essential for assessing the protective effects and elucidating the action mechanisms of TCM against KYDS, contributing significantly to research in this field. Research suggests that metabolomics and transcriptomics are effective in identifying biomarkers, targets, and metabolic pathways associated with TCM syndromes [16,17]. Following this identification, molecular validation, particularly using reverse-transcription quantitative real-time polymerase chain reaction (RT-qPCR) analysis, can provide detailed insights into the specific mechanism of action of TCM therapies. In line with this approach, in the present study, we aim to employ metabolomics and transcriptomics, supplemented by RT-qPCR validation methods, to systematically investigate the underlying mechanisms by which BGZ exerts its therapeutic effects in the treatment of KYDS.

2. Materials and methods

2.1. Chemicals and reagents

Hydrocortisone was sourced from Tianjin Biochemical Pharmaceutical Co., Ltd. (Tianjin, China, 022,003,012). Reagents for alanine aminotransferase (ALT), aspartate aminotransferase (AST), and alkaline phosphatase (ALP) assays were procured from Jiancheng Biological Technology, Co., Ltd. (Nanjing, China). Adrenocorticotropic hormone (ACTH), corticosterone (CORT), 17-hydroxycorticosteroids (17-OHCS), triiodothyronine (T3), thyroxine (T4), thyrotropin (TSH), cyclic adenosine monophosphate (cAMP), cyclic guanosine monophosphate (cGMP), and testosterone (T) were obtained from Mlbio Biotechnology Co., Ltd. (Shanghai, China).

2.2. BGZ preparation

BGZ was procured from Anhui Puren Herbal Pieces Co., Ltd. (Anhui, China, 2,102,062), with its authenticity verified by Professor Jin-Fa Tang of the Department of Pharmacy, the First Affiliated Hospital of Henan University of Traditional Chinese Medicine (Zhengzhou, China). BGZ powder was ground using a grinder and sieved through a 200-mesh sieve for administration. The BGZ extract was prepared following the 2020 edition of the Chinese Pharmacopoeia Commission [8]. Briefly, 0.5 g of dried BGZ was finely ground and subjected to heat reflux extraction for 2 h with 100 mL methanol using a Soxhlet extractor. The extract was then filtered, and the resulting filtrate was collected for further use.

2.3. Ultra-high performance liquid chromatography (UPLC) with ultraviolet analysis

Ultra-high performance liquid chromatography (UPLC) was employed to identify the presence of psoralen and isopsoralen in the BGZ extract. Psoralen and isopsoralen standards were purchased from Chengdu Pufei De Biotech. UPLC-grade solvents, including methanol (CH_3OH) and acetonitrile (CH_3CN) (Merck KGaA, Germany) were used. The analysis was performed on a Waters Acquity UPLC H-Class apparatus equipped with an Empower 2 chromatography workstation. The mobile phase consisted of mobile phase A (CH_3CN) and mobile phase B (CH_3OH), with the following gradient: 0–6 min 50 % A and 50 % B. The UPLC was conducted at 25 °C for the sample and 30 °C for the column, with a flow rate of 0.2 mL/min on an Inno C-18 (150 mm × 4.6 mm, 5 μm, Waters symmetry), and an injection volume of 1 μL. Ultraviolet spectra were recorded at a wavelength of 246 nm.

2.4. Animal treatment

Male Sprague–Dawley rats (180–200 g) were procured from SPF Biotechnology Co. Ltd. (License No. SCXK20190010, Beijing, China) and housed in the Laboratory Animal Center of the Fifth Medical Centre, Chinese PLA General Hospital, under specific pathogen-free conditions. The study received approval from the animal ethics committee (No. YFYDW2020017). The rats were maintained on a 12-h light/dark cycle with unrestricted access to appropriate food and water.

The rats were randomly assigned to six groups (n = 8) using the random number table method (Table 1), with each group receiving specific treatments: 0.5 % sodium carboxymethylcellulose (CMC-Na) administration (CON group); BGZ_L powder at a dosage of 0.9 g/kg (BGZ_L group); BGZ_H powder at a dosage of 2.7 g/kg (BGZ_H group); hydrocortisone at 25 mg/kg (KYDS group); BGZ_L powder at 0.9 g/kg and hydrocortisone at 25 mg/kg (KYDS + BGZ_L group); and BGZ_H powder at 2.7 g/kg and hydrocortisone at 25 mg/kg (KYDS + BGZ_H group). The CON and KYDS groups received a daily gavage of 0.5 % sodium carboxymethyl cellulose (CMC-Na), while the remaining groups received the respective BGZ dosage continuously for 21 consecutive days. The BGZ dosages were determined based on the methodology established by Hee-Sok Jun [18]. From the 8th day of administration, the KYDS group received a subcutaneous injection of hydrocortisone at a dosage of 25 mg/kg once daily for a subsequent 14 days to induce the KYDS model [19]. Changes in body weight were recorded until the conclusion of the experiment.

2.5. Blood collection, organ index, and tissue preparations

Upon completion of the experiment, animals were anesthetized, and serum samples were collected for liver function, hormone, and neurotransmitter analyses. The liver and kidneys were then excised and weighed, with the liver immediately fixed in 4 % paraformaldehyde for subsequent pathological assessments. The remaining liver tissue was reserved for metabonomic analysis.

2.6. Serum biochemistry and histopathological analysis

Following centrifugation at 3500 rpm for 10 min at 4 °C, serum biochemistry parameters including ALT, AST, and ALP, along with hormone levels (ACTH, CORT, 17-OHCS, T3, T4, TSH, T), and neurotransmitters (cAMP and cGMP), were quantified according to the respective microplate assay kit protocols. The larger left lobe of the liver was preserved in paraffin, sectioned at approximately 5 μm thickness, and subjected to hematoxylin and eosin (HE) staining for histopathological analysis.

2.7. RNA sequencing analysis and data processing

Total RNA was extracted from liver tissue using Trizol reagent (Invitrogen, USA), and the quality of the samples was assessed using a bioanalyzer 2100 (Agilent) and quantified with a NanoDrop 2000 spectrophotometer. Only samples meeting the following criteria were included in the sequencing library preparation: RNA integrity number (RIN) ≥ 6.5, 28S:18S ≥ 1.0, OD260/280 = 1.8–2.2, OD260/230 ≥ 2.0, and RNA quantity exceeding 1 μg. RNA-seq transcriptome libraries were prepared using the TruSeqTMRNA sample preparation Kit (San Diego, CA) and sequenced on an Illumina HiSeq xten/NovaSeq 6000 sequencer. The quality of sequencing was ensured with a Q30 (bases of Q ≥ 30/all bases of sequencing) exceeding 91 %. Sequence reads were trimmed and underwent quality control processes employing SeqPrep (https://github.com/jstjohn/SeqPrep) and Sickle (https://github.com/najoshi/sickle). The reads were aligned to the GRCm39 reference genome (http://asia.ensembl.org/Mus_musculus/Info/Index) using HISAT2 Version 2.1.0 (http://ccb.jhu.edu/software/hisat2/index.shtml) in localization mode [20]. Differentially expressed genes (DEGs) were

Table 1
Animal grouping and treatment.

Group	Treatment
CON	–
BGZ_L	0.9 g/kg BGZ (21 days)
BGZ_H	2.7 g/kg BGZ (21 days)
KYDS	25 mg/kg hydrocortisone (14 days)
KYDS + BGZ_L	0.9 g/kg BGZ (21 days)+ 25 mg/kg hydrocortisone (14 days)
KYDS + BGZ_H	2.7 g/kg BGZ (21 days)+ 25 mg/kg hydrocortisone (14 days)

identified by calculating transcript expression levels using the transcript per million reads (TPM) method with Z-score standardization. Quantification of messenger RNA levels was performed using RSEM [21], and differential expression analysis was conducted by filtering for $|\mathrm{Log_2}(\text{fold change})| > 1$ and $Padjust < 0.05$ to identify differentially expressed genes (DEGs) [22].

2.8. Liver sample processing

Liver tissue was homogenized with normal saline at a 1:1 ratio (1 g tissue: 1 mL saline) at 4 °C. The resulting homogenate was mixed with methanol at a 1:3 ratio and vortexed for 30 s. The supernatant was then centrifuged at 12,000 revolutions per minute (r/min) for 10 min and concentrated to dryness using a vacuum-refrigerated centrifugal concentrator. The dried sample was redissolved in 100 μL of methanol and subjected to additional centrifugation at 13,000 r/min for 10 min. The final supernatant was analyzed using ultra-performance liquid chromatography coupled with quadrupole/time-of-flight mass spectrometry (UPLC-QTOF/MS) detection on a Waters system (Manchester, UK).

2.9. UPLC-QTOF/MS analysis and data processing

A 4 μL aliquot of each sample was injected into an Acquity UPLC HSS T3 C18 analytical column, maintained at 30 °C. During the positive/negative electrospray ionization source analysis, separation was achieved using mobile phase A (0.1 % formic acid in water) and mobile phase B (0.1 % formic acid in acetonitrile) at a flow rate of 0.30 mL/min. To ensure system stability and repeatability, 10 μL from each sample was pooled to create a quality control sample, which was injected into the system every 20 samples during analysis. Accurate mass determination was performed using leucine enkephalin (ESI-m/z 554.2615, ESI + m/z 556.2771) as the lock mass solution.

Metabolic profiling of biofluids was executed carried out using the Waters Xevo G2-XS QTOF/MS system. Initial mass spectral data were processed and normalized for total ion intensity using Masslynx software (Waters Corp.) and Progenesis QI (v. 2.4, Waters Technologies, UK), with reference to leucine enkephalin. This generated a data matrix comprising m/z values, retention times (RT), and normalized peak areas. Principal component analysis (PCA) and orthogonal partial least-squares discriminant analysis (OPLS-DA) were performed using SIMCA-P 14.1 software (Umetrics, Umea, Sweden). For metabolite selection, a coefficient was established based on the variable importance in the projection (VIP) value ≥ 1 and $p\text{-}value < 0.05$ determined by the T-test comparing the means of two samples. Differential metabolites were identified using online databases such as the Human Metabolome Database (HMDB) (http://www.hmdb.ca/) and Kyoto Encyclopedia of Genes and Genomes (KEGG) (https://www.genome.jp/kegg/). The exact masses and secondary ion mass spectrometry data obtained through Progenesis QI were cross-referenced with these databases for comprehensive identification.

2.10. Reverse-transcription quantitative real-time polymerase chain reaction (RT-qPCR)

Total RNA was extracted from liver tissue using the Tissue RNA Purification Kit Plus, according to the manufacturer's instructions (RN002plus, ES Science, China). The isolated RNA was reverse-transcribed into complementary DNA (cDNA) using the Fast All-in-One RT Kit (RT001, ES Science, China) following standard protocols. The qPCR assay was conducted using the SYBR Green PCR master mix (RN002plus, ES Science, China) on the QuantStudio 6 Flex PCR System (Applied Biosystems, USA). Amplification parameters included an initial denaturation at 95 °C for 30 s, followed by 40 cycles of denaturation at 95 °C for 5 s, and annealing/extension at 60 °C for 34 s. A final extension was performed at 95 °C for 15 s, followed by annealing at 60 °C for 60 s, and a final denaturation at 95 °C for 15 s. The relative expression levels of mRNA were normalized to their corresponding Gapdh mRNA levels. Primer sequences are provided in Supplemental Table 1. Quantification was performed using the $2^{-\Delta\Delta Ct}$ method [23].

2.11. Molecular docking

Molecular docking analysis was performed using Maestro 11.0 software. The crystal structures of the selected protein targets were obtained from the RCSB Protein Data Bank (http://www.pdb.org/). These structures underwent preparation steps, including the addition of ligands and water, the addition of hydrogen, the optimization of amino acids, and overall structural optimization to minimize energy. Ligands associated with BGZ were obtained from the ETCM database (http://www.tcmip.cn/ETCM/index.php/Home/) [24]. The SDF format of these ligands was obtained from the PubChem database (https://pubchem.ncbi.nlm.nih.gov/), and the structures were optimized for energy minimization, rendering them suitable for the docking procedure. The original ligand in the receptor protein complex was removed, and the binding pocket size was determined to establish the molecular docking parameters. The XP method was used to conduct molecular docking.

2.12. Statistical analysis

All data are presented as mean ± SD and were analyzed using Prism 8.0 (GraphPad Software, San Diego, CA). For multiple-group comparisons, one-way ANOVA followed by Bonferroni's multiple comparisons test was employed. Student's t-test was utilized for analyzing receiver operating characteristic (ROC) curves, differential expression of metabolites, and DEGs. Spearman's correlation analysis was conducted to assess the relationship between DEGs and serum biochemistry, as well as between differential metabolites and serum biochemistry. A significance level of $P < 0.05$ was considered statistically significant.

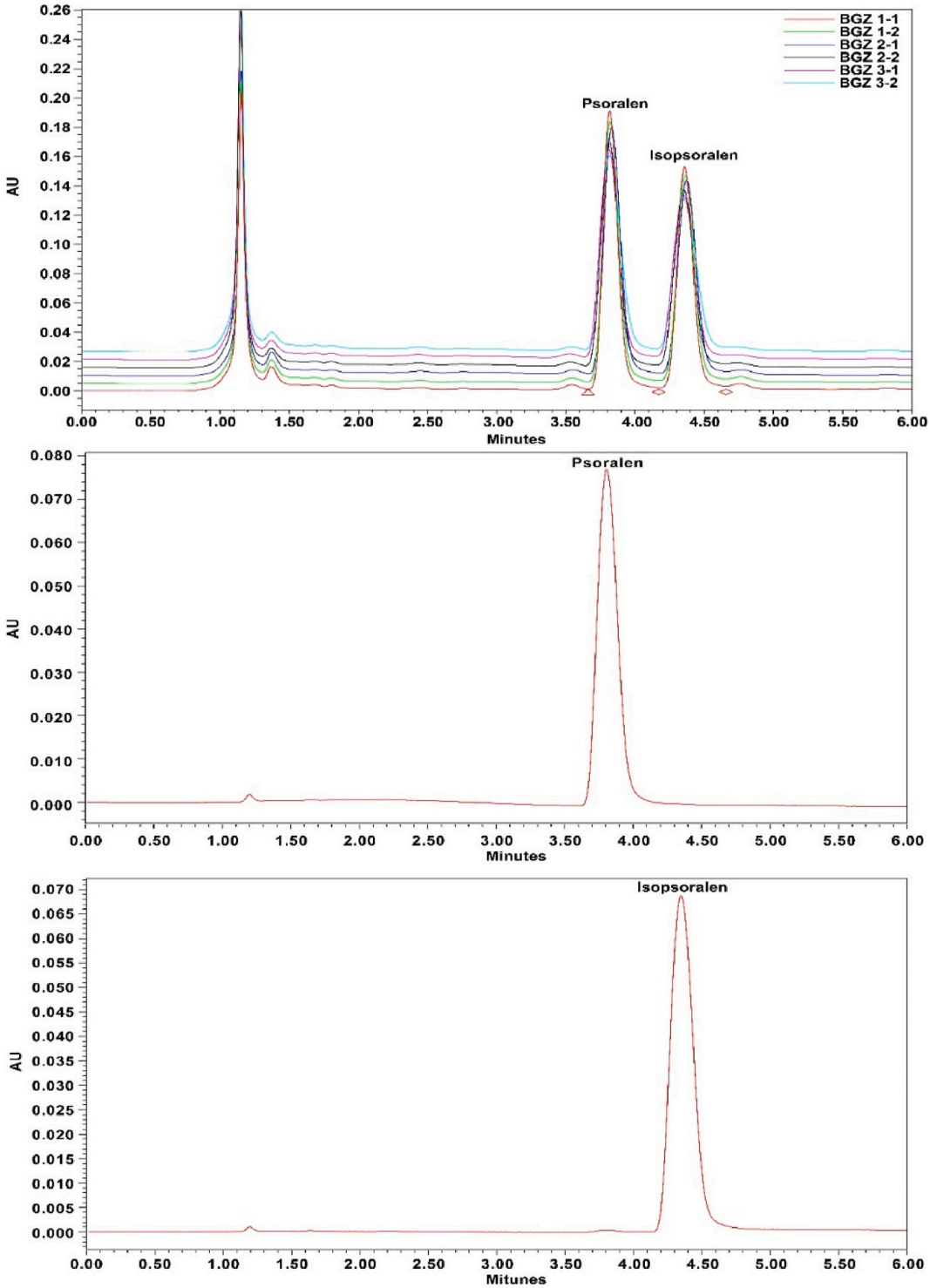

Fig. 1. UPLC with ultraviolet analysis for psoralen and isopsoralen. UPLC with ultraviolet analysis was conducted using psoralen (0.05 mg/mL), isopsoralen (0.05 mg/mL), and BGZ extract (10 mg/mL). UV spectra were obtained for each compound and BGZ extract.

3. Results

3.1. Identification of psoralen and isopsoralen in the BGZ extract

Psoralen and isopsoralen were identified in the BGZ extract using ion chromatography, with retention times of 3.8 and 4.6 min, respectively. The presence of these compounds was further confirmed through their UV spectra, as illustrated in Fig. 1.

3.2. Effects of BGZ treatment on rectal temperature, body weight, and organ indexes in KYDS rats

As shown in Table 2, the KYDS group exhibited a significant reduction in rectal temperature compared to the CON group ($P < 0.05$), confirming the successful induction of the KYDS model. Treatment with both low-dose (BGZ_L) and high-dose (BGZ_H) BGZ resulted in a significant increase in rectal temperature in the KYDS rats compared to the untreated KYDS group (both $P < 0.05$), suggesting that BGZ may alleviate the hypothermic condition associated with KYDS.

Regarding body weight, there were no significant differences between the BGZ_L group and the KYDS group when compared to the CON group. However, both the BGZ_H group and the KYDS + BGZ_H group exhibited a significant decrease in body weight (both $P < 0.01$). Additionally, no statistically significant changes were observed in hepatic, renal, and testicular indices in the BGZ_L group and the KYDS + BGZ_L group when compared to the CON group and KYDS group, respectively. Notably, the BGZ_H group demonstrated a significant increase in hepatic, renal, and testicular indices compared to the CON group ($P < 0.001$, $P < 0.001$, $P < 0.01$, respectively). Interestingly, while the KYDS + BGZ_H group showed significant increases in hepatic and testicular indices compared to the KYDS group, there were no statistically significant differences when compared to the BGZ_H group alone. These findings suggest that high-dose BGZ administration may carry a potential risk of hepatic, renal, and testicular damage.

3.3. Effects of BGZ treatment on serum biochemistry and histopathology in KYDS rats

Serum levels of ALT, AST, and ALP were assessed as indicators of liver function. As illustrated in Fig. 2A–C, no significant differences were observed in ALT, AST, and ALP in the BGZ groups (BGZ_L and BGZ_H) compared to the CON group. In contrast, the KYDS group showed a significant reduction in ALT and AST levels following BGZ_L treatment ($P < 0.001$ for both). However, the KYDS + BGZ_H group exhibited significant increases in AST and ALP levels compared to the CON group ($P < 0.001$ for both).

Histopathological examination, depicted in Fig. 2D, revealed that liver samples from BGZ_L-treated rats were nearly indistinguishable from those of the CON group, while BGZ_H-treated rats showed mild inflammatory infiltration in the portal area without apparent hepatocyte injury. In the KYDS group, liver samples displayed signs of hepatocyte focal necrosis, loss of central vein intima, and inflammatory cell infiltration in the portal areas. These pathological features were notably alleviated in the KYDS + BGZ_L group. However, the KYDS + BGZ_H group exhibited more severe hepatocyte focal necrosis and extensive inflammatory infiltration compared to the KYDS + BGZ_L group.

Kidney histology, as shown in Fig. 2E, indicated that the glomeruli in the CON, KYDS, KYDS + BGZ_L, and KYDS + BGZ_H groups retained regular morphology with clear contours, and no significant signs of inflammatory infiltration or pathological alterations were observed.

Collectively, the results of ALT, AST, ALP levels, and liver histopathology suggest that BGZ_L exerts a significant hepatoprotective effect in KYDS rats, whereas BGZ_H does not demonstrate clear hepatoprotective efficacy and may even induce hepatic damage. Due to the potential risk of liver and kidney damage, only low doses of BGZ (0.9 g/kg) were used in subsequent studies.

Table 2
Table of changes in body weight and liver, kidney, and testicular organ index.

Group	Rectal temperature	Body weight (g)	Liver		Kidney		Testicular	
			Weight	Index (%)	Weight	Index (%)	Weight	Index (%)
CON	36.46 ± 0.13	319.76 ± 20.85	8.27 ± 0.87	2.64 ± 0.12	2.07 ± 0.24	0.62 ± 0.03	3.13 ± 0.27	0.98 ± 0.08
BGZ_L	36.30 ± 0.38	321.39 ± 15.00	9.39 ± 0.69	2.89 ± 0.12	2.20 ± 0.18	0.67 ± 0.04	3.13 ± 0.28	0.98 ± 0.10
BGZ_H	36.59 ± 0.35	281.70 ± 26.96**	11.05 ± 1.09	3.94 ± 0.45***	2.15 ± 0.16	0.76 ± 0.05***	2.88 ± 0.70	1.10 ± 0.10**
KYDS	35.94 ± 0.25*	312.04 ± 21.56	9.68 ± 1.16	3.14 ± 0.17*	2.26 ± 0.25	0.72 ± 0.08**	3.12 ± 0.26	1.00 ± 0.11
KYDS + BGZ_L	36.19 ± 0.31$^{\#}$	313.59 ± 17.84	10.61 ± 1.09	3.29 ± 0.24	2.25 ± 0.15	0.72 ± 0.06	3.16 ± 0.13	1.01 ± 0.08
KYDS + BGZ_H	36.79 ± 0.69$^{\#\#}$	276.99 ± 16.61$^{\#\#}$	12.03 ± 1.20	4.27 ± 0.49$^{\#\#\#}$	2.14 ± 0.27	0.76 ± 0.04	3.09 ± 0.23	1.12 ± 0.09$^{\#\#}$

*$P < 0.05$, ***$P < 0.01$, ***$P < 0.001$, compared with that in the CON group; $^{\#\#}P < 0.01$, $^{\#\#\#}P < 0.001$, compared with that in the KYDS group.

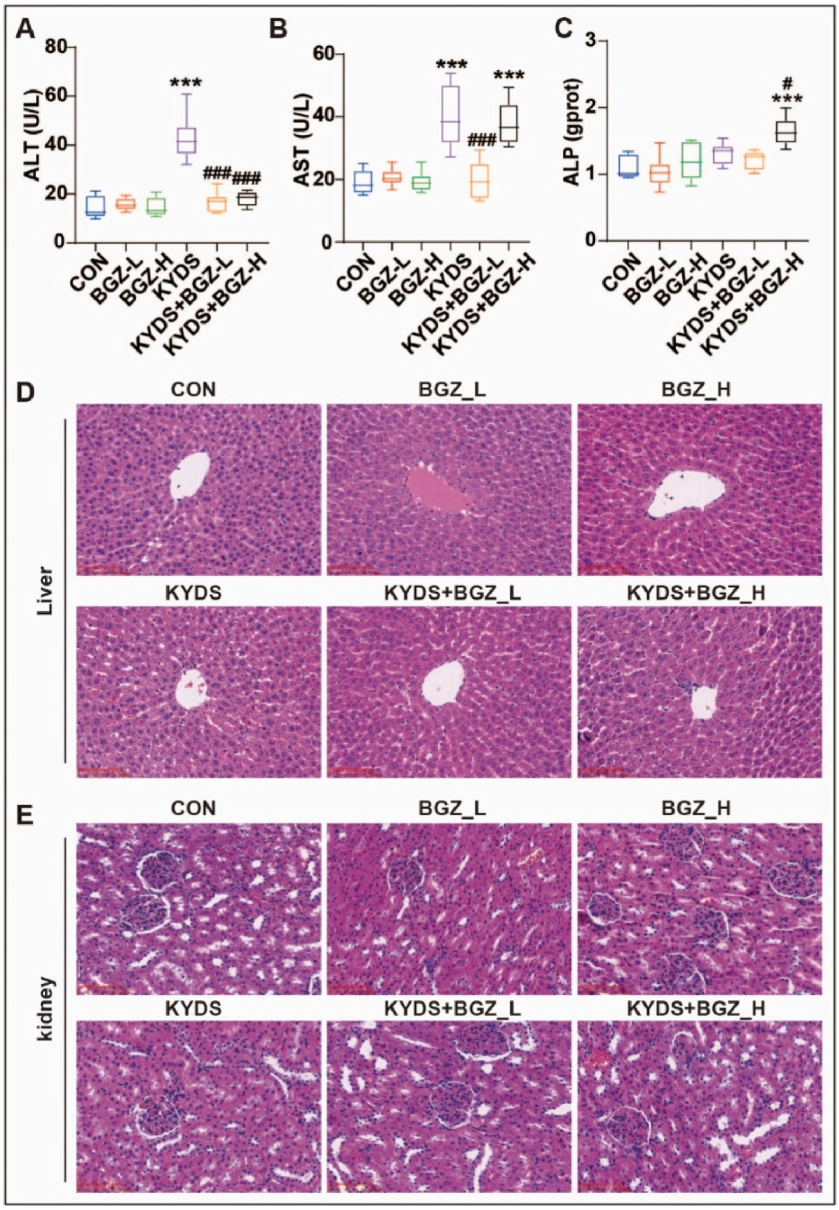

Fig. 2. Effect of BGZ treatment on serum biochemistry and histopathological examination in KYDS rats (N = 8). Serum ALT (A), AST (B), and ALP (C) activity in rats co-treated with BGZ_L (0.9 g/kg), or BGZ_H (2.7 g/kg) (normal rats or KYDS rats). $^{***}P < 0.001$, compared with CON group; $^{\#}P < 0.05$, $^{\#\#\#}P < 0.001$, compared with KYDS group. (D–E) HE pathological staining of liver tissue (D) and kidney tissue (E) (Scale bar, 100 μm).

3.4. Transcriptomic alterations induced by BGZ treatment in KYDS rats

To explore the mechanisms through which BGZ (0.9 g/kg) alleviates liver injury in KYDS rats, liver gene expression profiles were obtained from the CON group, BGZ group, KYDS group, and KYDS + BGZ group through RNA-Seq analysis. As shown in Fig. 3A, PCA analysis revealed that the BGZ group was not significantly different from the CON group, while the KYDS group was clearly distinguishable from the CON group. Additionally, the KYDS + BGZ group was distinguishable from the KYDS group. As depicted in Fig. 3B, BGZ treatment had minimal impact on gene expression compared to the CON group, with only 4 DEGs upregulated and 5 DEGs downregulated. In contrast, the KYDS group showed substantial changes, with 419 DEGs upregulated and 623 DEGs downregulated. However, with BGZ treatment, the number of upregulated and downregulated DEGs decreased to 38 and 54, respectively, compared to the KYDS group. A Venn diagram illustrating the DEG profiles identified 25 DEGs influenced by BGZ, suggesting potential liver protection. This was discerned by identifying the intersecting DEGs among the CON, KYDS, and KYDS + BGZ groups (Fig. 3C–Supplemental Table 2). A heatmap was generated to visualize the relative abundance of DEGs specifically altered by BGZ

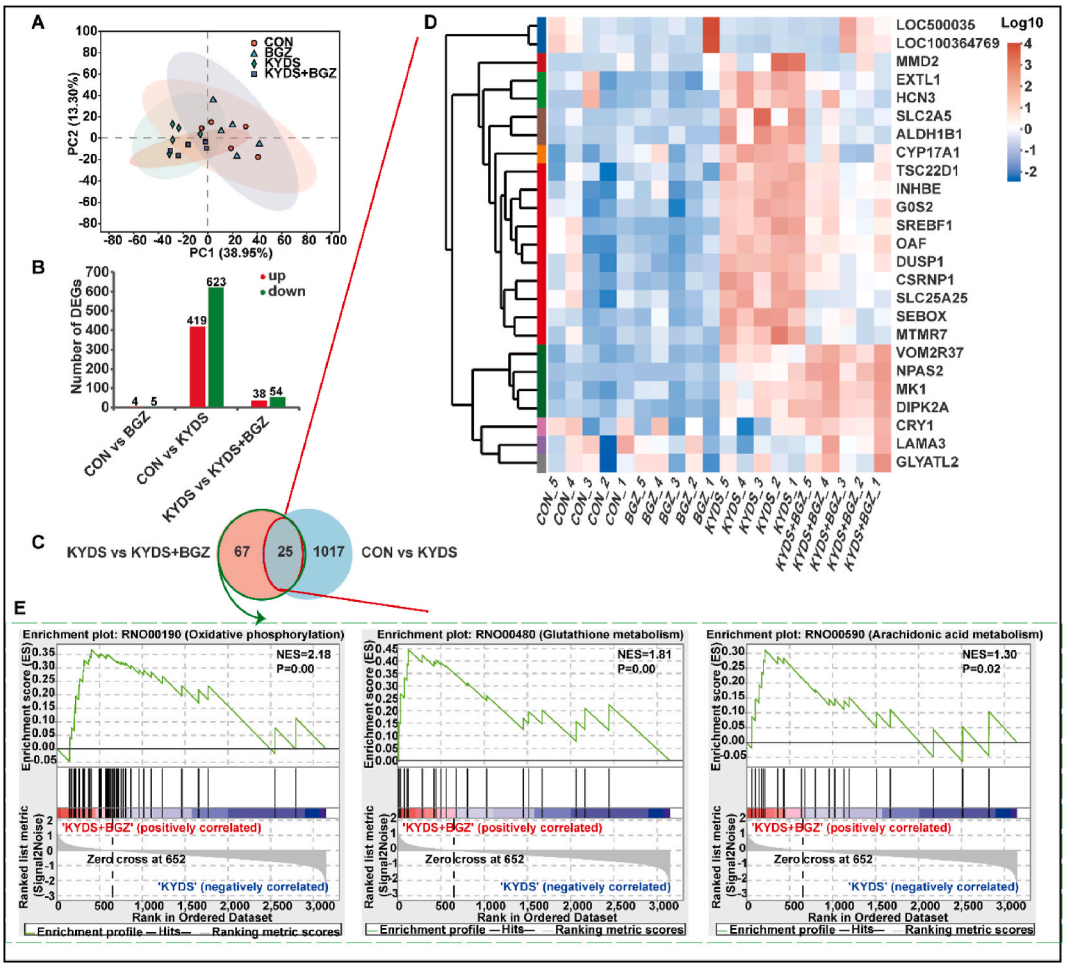

Fig. 3. Transcriptomic analysis of liver tissues in the groups of CON, BGZ (0.9 g/kg), KYDS, and KYDS + BGZ (0.9 g/kg) (N = 5). (A) PCA analysis between different groups. (B) The number of DEGs compared with each group, the red color represents an up-regulated gene and the green color represents the down-regulated gene. (C) Venn diagram of DEGs compared among the groups of CON, KYDS, and KYDS + BGZ. Heatmap (D) and GSEA (E) analysis the DEGs specifically changed by BGZ in KYDS rats which is different from Changes in normal rats. NES: Normalized enrichment score.

(Fig. 3D). Gene set enrichment analysis (GSEA) indicated that DEGs affected by BGZ were predominantly enriched in pathways related to oxidative phosphorylation (OXPHOS), glutathione metabolism, and arachidonic acid metabolism (Fig. 3E).

3.5. *Correlation analysis between DEGs and serum biochemistry*

Correlation analysis between serum biochemical parameters (ALT, AST, and ALP) and DEGs (Fig. 4A) revealed a significant positive correlation between ALT and several genes, including dual specificity phosphatase 1 (*DUSP1*), inhibin subunit beta E (*INHBE*), G0/G1switch 2 (*G0S2*), sterol regulatory element binding transcription factor 1 (*SREBF1*), exostosin-like glycosyltransferase 1 (*EXTL1*), solute carrier family 25 member 25 (*SLC25A25*), SEBOX homeobox (*SEBOX*), hyperpolarization-activated cyclic nucleotide-gated potassium channel 3 (*HCN3*), cysteine and serine rich nuclear protein 1 (*CSRNP1*), cytochrome P450 family 17 subfamily A member 1 (*CYP17A1*), myotubularin related protein 7 (*MTMR7*), solute carrier family 2 member 5 (*SLC2A5*), out at first homolog (*OAF*), and *TSC22* domain family member 1 (*TSC22D1*) (all $r > 0.50$). A negative correlation was observed with LRRG00136-like (*LOC100364769*) ($r < -0.50$). AST was significantly positively correlated with *HCN3*, *EXTL1*, *CYP17A1*, *SEBOX*, *INHBE*, and *MTMR7* (all $r > 0.50$). ALP was significantly positively correlated with *OAF*, *CSRNP1*, *SLC2A5*, *DUSP1*, *SREBF1*, *MTMR7*, *TSC22D1*, *G0S2*, *NPAS2*, aldehyde dehydrogenase 1 family member B1 (*ALDH1B1*), divergent protein kinase domain 2A (*DIPK2A*), *SLC25A25*, and Mk1 protein (*MK1*) (all $r > 0.50$). Among these, *MTMR7* and *TSC22D1* were positively correlated with ALT, AST, and ALP. The correlation coefficients (r) and *P-value* are detailed in Supplemental Table 3. Validation through RT-qPCR confirmed the significant inhibitory effects of BGZ on the expression of *MTMR7*, *TSC22D1*, *ALDH1B1*, *DUSP1*, *CSRNP1*, and *CYP17A1* in KYDS rats (all $P < 0.05$) (Fig. 4B–G).

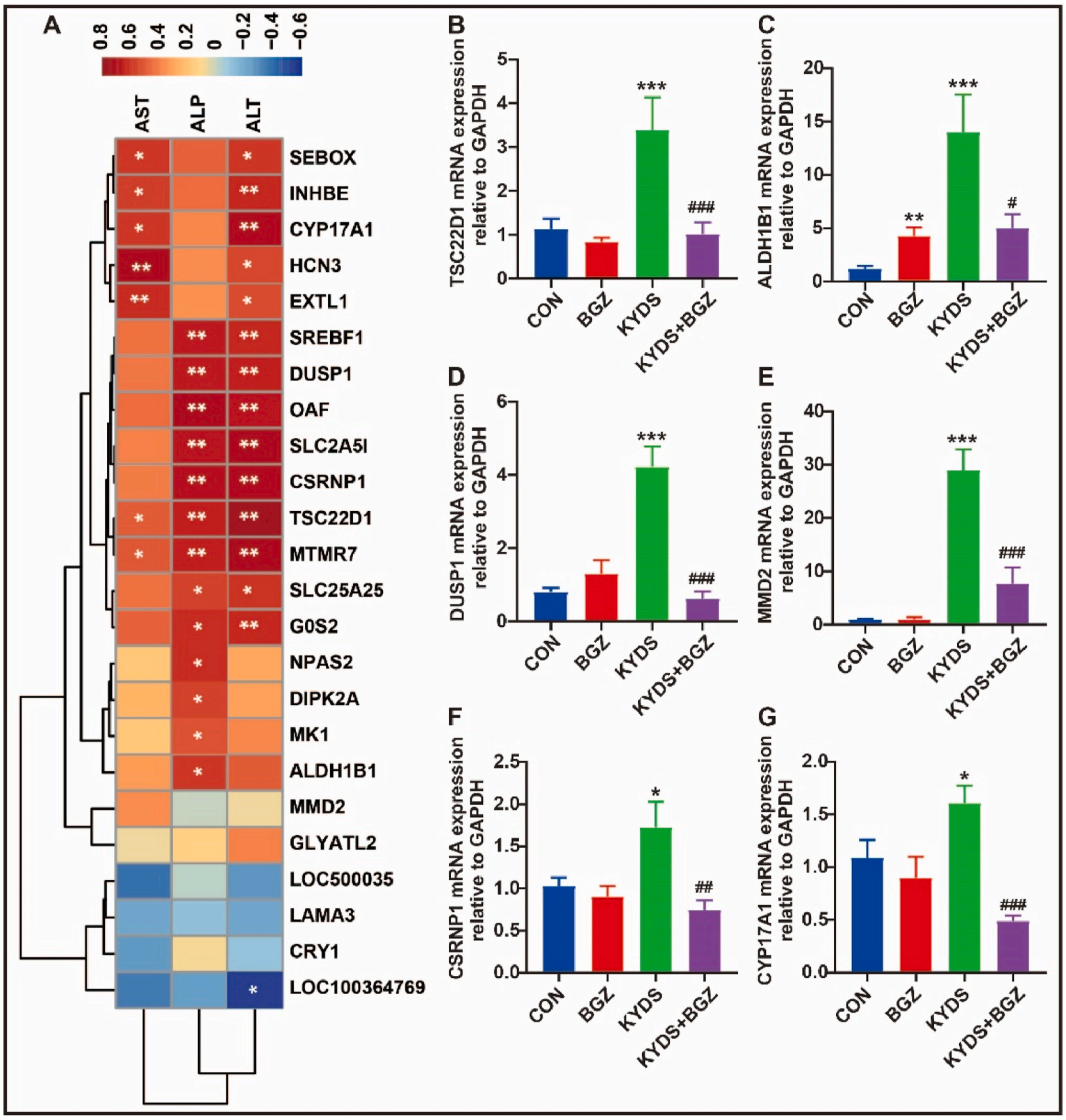

Fig. 4. The relationship between DEGs and serum biochemistry. (A) Heatmap of the correlation between serum biochemistry and DEGs (N = 5), color depth represents correlation strength, yellow color represents positive correlation, blue color represents negative correlation, $^{*}P < 0.05$, $^{**}P < 0.01$, $^{***}P < 0.001$. (B ~ G) 6 related differential genes verified by RT-qPCR (N = 8). $^{*}P < 0.05$, $^{***}P < 0.001$, compared with CON group; $^{\#}P < 0.05$, $^{\#\#}P < 0.01$, $^{\#\#\#}P < 0.001$, compared with KYDS group.

3.6. Liver metabolomics analysis of BGZ treatment in KYDS rats

As shown in Fig. 5A–B, the quality control (QC) samples clustered tightly in both PCA score plots, signifying the stability of the UPLC-QTOF/MS system throughout the analysis. In the automated simulation process, six principal components were identified in electrospray positive ion (ESI+) mode ($R^2X = 0.618$), while five principal components were identified in electrospray negative ion (ESI-) mode ($R^2X = 0.58$). The samples largely fell within the 95 % confidence interval (CI) represented by the Hotelling T2 ellipse. Distinct separations were observed among the CON, BGZ, KYDS, and KYDS + BGZ groups, indicating metabolic differences between these groups.

OPLS-DA demonstrated effective separation between the CON group and KYDS group (Fig. 5C–D) as well as between the KYDS group and KYDS + BGZ group (Fig. 5E–F) in both the ESI+ and ESI- modes. Permutation tests for OPLS-DA (Supplemental Fig. 1) confirmed that the models were not overfitted. These findings suggest significant metabolic disturbances in the KYDS group compared to the CON group and further alterations in the KYDS + BGZ group compared to the KYDS group. A comprehensive analysis revealed 20 metabolites exhibiting differences between the KYDS + BGZ group and the KYDS group, characterized by their *m/z* values and secondary fragment ion features (Table 3). Supplementary Fig. 2 provides detailed characteristic maps of secondary fragment ions for the identified metabolites. The heatmap depicting the variations in the aforementioned differential metabolites is shown in Fig. 6. The

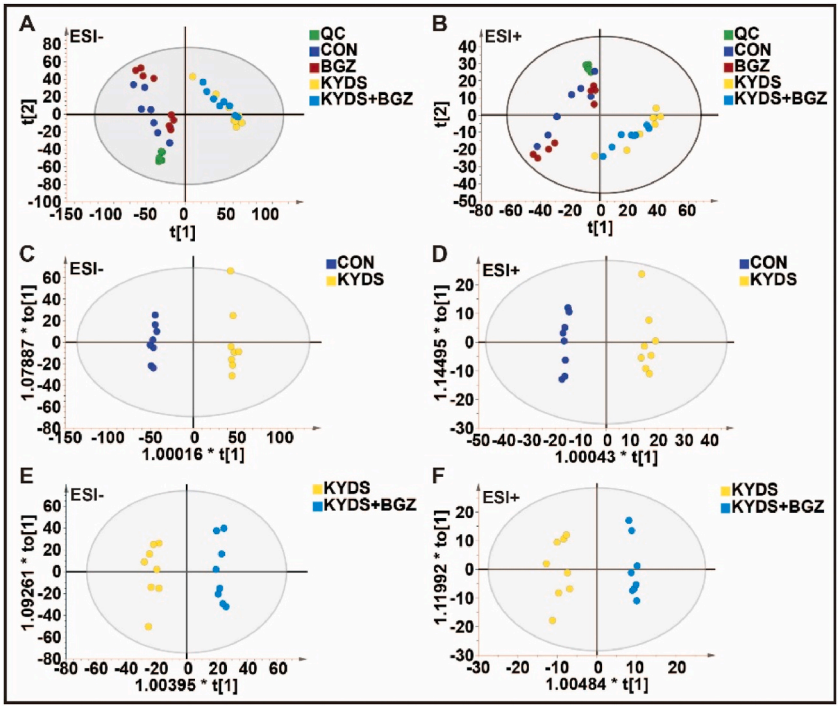

Fig. 5. Metabolomic analysis of liver tissue in CON group, BGZ group (0.9 g/kg), KYDS group, and KYDS + BGZ group (0.9 g/kg) (N = 8). (A–B) Scores scatter plot of liver metabolites in all groups determined by principal component analysis (PCA) in electrospray ionization source negative (ESI-) mode (A) and electrospray ionization source positive (ESI+) mode (B). (C–D) Scores scatter plot of liver metabolites in the CON and KYDS groups determined by orthogonal partial least-squares discriminant analysis (OPLS-DA) in ESI- mode (C) and ESI + mode (D). (E–F) Scores scatter plot of liver metabolites in the KYDS and KYDS + BGZ groups determined by OPLS-DA in ESI- mode (E) and ESI + mode (F).

Table 3
Identified differential metabolites among the CON group, KYDS group, and KYDS + BGZ group.

Number	RT (min)	*m/z*	Metabolites	KEGG	Trends		
					BGZ vs CON	KYDS vs CON	(KYDS + BGZ) vs KYDS
ESI-							
1	0.75	384.1438	4-(Methylnitrosamino)-1-(3-pyridyl)-1-butanol glucuronide	C19605	↑	↓***	↑**
2	0.82	184.0007	O-Phospho-L-serine	C01005	↑	↓***	↑*
3	0.94	145.0132	Oxoglutaric acid	C00026	↓	↓**	↑*
4	1.31	116.0708	L-Valine	C00183	↑	↓***	↑*
5	1.39	148.0378	Pyridoxal	C00250	↑	↓*	↑*
6	1.63	450.1319	(1S)-Hydroxy-(2S)-glutathionyl-1,2-dihydronaphthalene	C14792	↑	↓*	↑*
7	11.69	397.2291	Prostaglandin E2	C00584	↓	↓***	↑*
8	13.71	577.3444	L-Urobilinogen	C05789	↓	↑**	↓*
9	13.89	679.572	1-Acyl-sn-glycero-3-phosphocholine	C04230	↓**	↓**	↑**
10	14.14	623.5026	Diacylglycerol	C00165	↑	↑*	↓*
11	2.15	990.2553	trans,cis-Lauro-2,6-dienoyl-CoA	C05279	↓	↓**	↑*
12	5.74	593.3338	L-Urobilin	C05793	↓	↑*	↓**
ESI+							
13	0.96	381.0794	N1-(5-Phospho-a-D-ribosyl)-5,6-dimethylbenzimidazole	C04778	↓*	↑*	↓*
14	1.29	276.1065	(−)-threo-Iso(homo)3-citrate	C16600	↓	↑*	↓*
15	1.55	188.0663	L-Phenylalanine	C00079	↓	↑*	↓*
16	1.89	372.0832	S-(Hercyn-2-yl)-L-cysteine S-oxide	C20994	↓	↑**	↓*
17	1.94	359.1032	Phosphopantetheine	C01134	↑	↑*	↓*
18	4.00	196.0943	D-Leucate	C03264	↑*	↓**	↑**
19	8.09	583.2554	Biliverdin	C00500	↑	↓**	↑**
20	9.29	481.2705	Leukotriene E4	C05952	↑	↓**	↑*

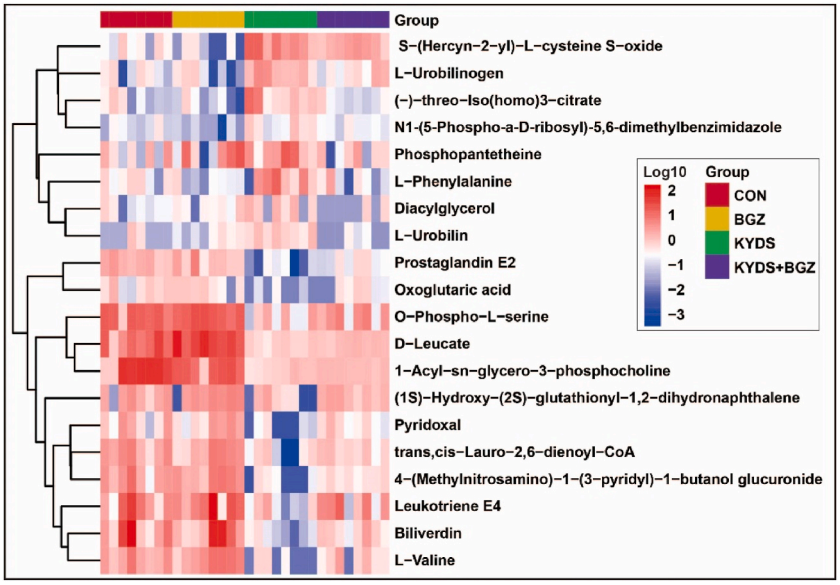

Fig. 6. Heatmap shows the intersection of identified metabolites among the groups of CON, KYDS, and KYDS + BGZ. Color depth represents the variation trend of relative abundance of metabolites, red color represents up-regulated metabolites, and blue color represents down-regulated metabolites.

association between metabolites and their corresponding metabolic pathways is shown in Supplementary Fig. 3.

3.7. Correlation analysis between identified metabolites and serum biochemistry

Correlation analysis between serum biochemistry parameters (ALT, AST, and ALP) and identified metabolites (Fig. 7) revealed a significant positive correlation was identified between ALT and L-Urobilinogen, S-(Hercyn-2-yl)-L-cysteine S-oxide, and (−)-threo-Iso (homo)3-citrate (all $r > 0.50$). Conversely, ALT exhibited a negative correlation with 4-(Methylnitrosamino)-1-(3-pyridyl)-1-butanol glucuronide, oxoglutaric acid, leukotriene E4, L-valine, prostaglandin E2, biliverdin, O-phospho-L-serine, and D-leucate (all $r < -0.50$). AST was positively correlated with (−)-threo-Iso(homo)3-citrate and S-(Hercyn-2-yl)-L-cysteine S-oxide (all $r > 0.50$) and negatively correlated with leukotriene E4, D-leucate, O-phospho-L-serine, prostaglandin E2, oxoglutaric acid, and 1-acyl-sn-glycero-3-phosphocholine (all $r < -0.50$). Furthermore, ALP displayed a significant positive correlation with L-urobilinogen, S-(Hercyn-2-yl)-L-cysteine S-oxide, and (−)-threo-Iso(homo)3-citrate (all $r > 0.50$) and a negative correlation with 4-(Methylnitrosamino)-1-(3-pyridyl)-1-butanol glucuronide, oxoglutaric acid, leukotriene E4, L-valine, prostaglandin E2, biliverdin, O-phospho-L-serine, and D-leucate (all $r < -0.50$). Among these metabolites, N1-(5-Phospho-α-D-ribosyl)-5,6-dimethylbenzimidazole, S-(Hercyn-2-yl)-L-cysteine S-oxide,

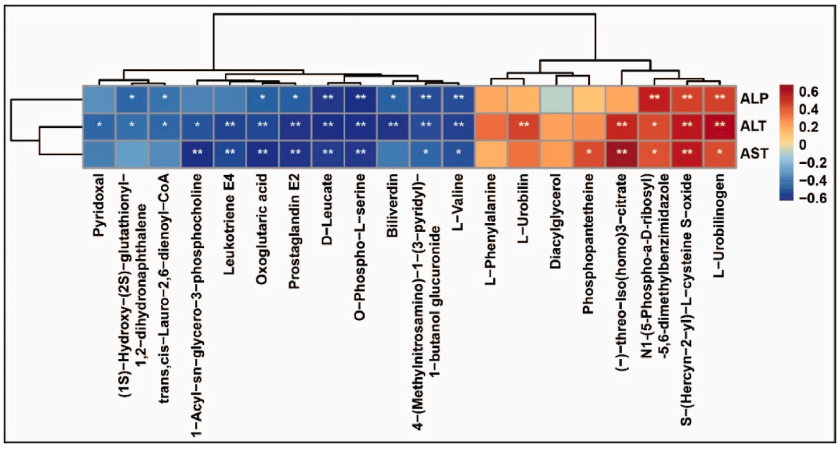

Fig. 7. The relationship between identified metabolites and serum biochemistry. (A) Heatmap of correlations between serum biochemistry and metabolites (N = 5), color depth represents correlation strength, yellow color represents positive correlation, blue color represents negative correlation, $*P < 0.05$, $**P < 0.01$.

and L-urobilinogen exhibited positive correlations with ALT, AST, and ALP. On the other hand, L-valine, 4-(Methylnitrosamino)-1-(3-pyridyl)-1-butanol glucuronide, O-phospho-L-serine, D-leucate, prostaglandin E2, and oxoglutaric acid displayed negative correlations with ALT, AST, and ALP. The correlation coefficients (r) and *P*-values are detailed in Supplemental Table 4.

3.8. ROC curve analysis of identified metabolites

To evaluate the diagnostic potential of the identified metabolites, ROC curve analysis was performed using GraphPad Prism software (version 8.01). As illustrated in Fig. 8A–E, 4-(Methylnitrosamino)-1-(3-pyridyl)-1-butanol glucuronide, biliverdin, L-urobilin, D-leucate, and (−)-threo-Iso(homo)3-citrate demonstrated strong discriminatory power between the KYDS and KYDS + BGZ groups, with all area under the ROC curve (AUC) values ≥ 0.90 and $P < 0.05$. These metabolites show promise as potential biomarkers for assessing the efficacy of BGZ in treating hydrocortisone-induced liver injury. The ROC curves for other identified metabolites, ranked by the AUC, are provided in Supplemental Fig. 4.

3.9. Network analysis of transcriptomics and metabolomics data

To investigate the comprehensive protective mechanism of BGZ in KYDS rats at a systemic level, a latent relationship network encompassing metabolites and DEGs altered by BGZ in KYDS rats was constructed using Metascape (www.metascape.org). The analysis identified 4 DEGs (CYP17A1, DUSP1, EXTL1, and ALDH1B1) and 7 metabolites (including Oxoglutaric acid, L-phenylalanine, Diacylglycerol, L-valine, Pyridoxal, Prostaglandin E2, O-phospho-L-serine). On this basis, the study conducted a correlation analysis between differential metabolites and DEGs and found a significant negative correlation between DUSP1 and pyridoxal ($r = -0.67$, $P < 0.03$). The correlation between these DEGs and metabolites is shown in Supplementary Fig. 5.

Given the identification of only 4 DEGs, constructing a comprehensive metabolite-gene-pathway network proved challenging, the study supplemented this analysis by incorporating genes associated with the identified metabolites according to the HMDB database. This integrated analysis revealed that the differentially expressed DEGs, metabolites, and associated genes predominantly clustered within pathways related to neuroactive ligand-receptor interaction, cAMP signaling, calcium signaling, cytokine-cytokine receptor interaction, and PI3K-AKT signaling (Fig. 9, Supplemental Table 5). This combined transcriptomic and metabolomic analysis offers valuable insights into the systemic protective mechanisms of BGZ in KYDS rats.

3.10. Alterations in cAMP signaling pathway in KYDS rats treated by BGZ

To validate the effects of BGZ on the cAMP signaling pathway, alterations in cAMP, cGMP, T3, T4, TSH, CORT, ACTH, and 17-OH-CS concentrations were measured using ELISA (Supplemental Fig. 5). Notably, BGZ significantly reversed the decreased expression of

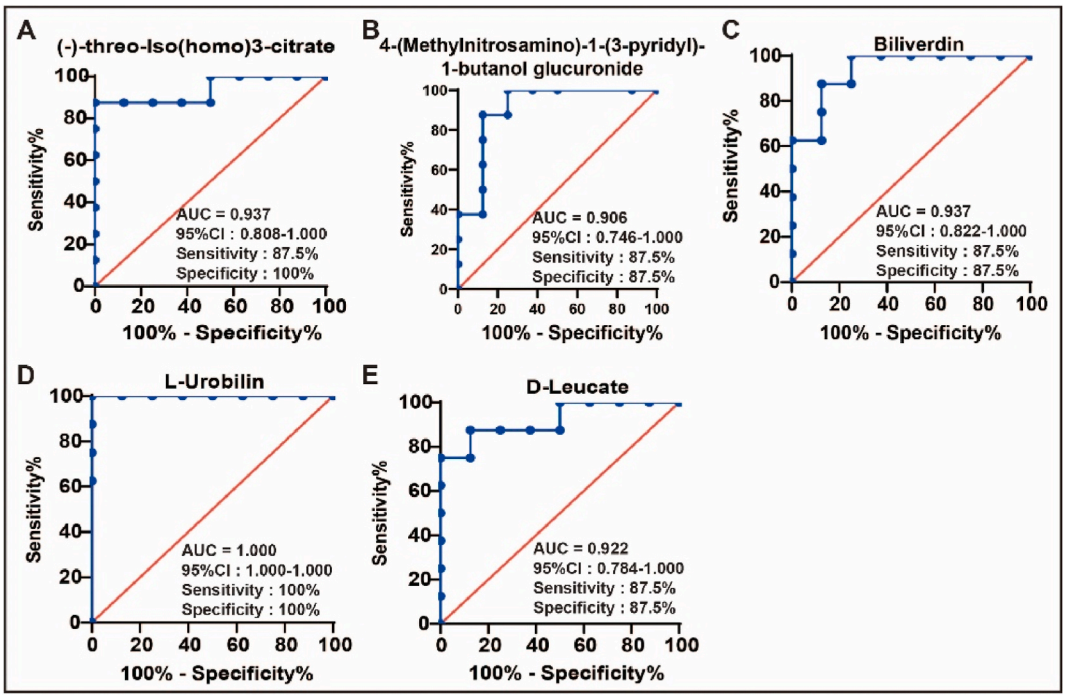

Fig. 8. ROC curves of identified metabolites (N = 8). (A) (−)-threo-Iso(homo)3-citrate, (B) 4-(Methylnitrosamino)-1-(3-pyridyl)-1-butanol glucuronide, (C) Biliverdin, (D) L-Urobilin, (E) D-Leucate. ROC: receiver operating characteristic, AUC: area under the ROC curve, CI: confidence interval.

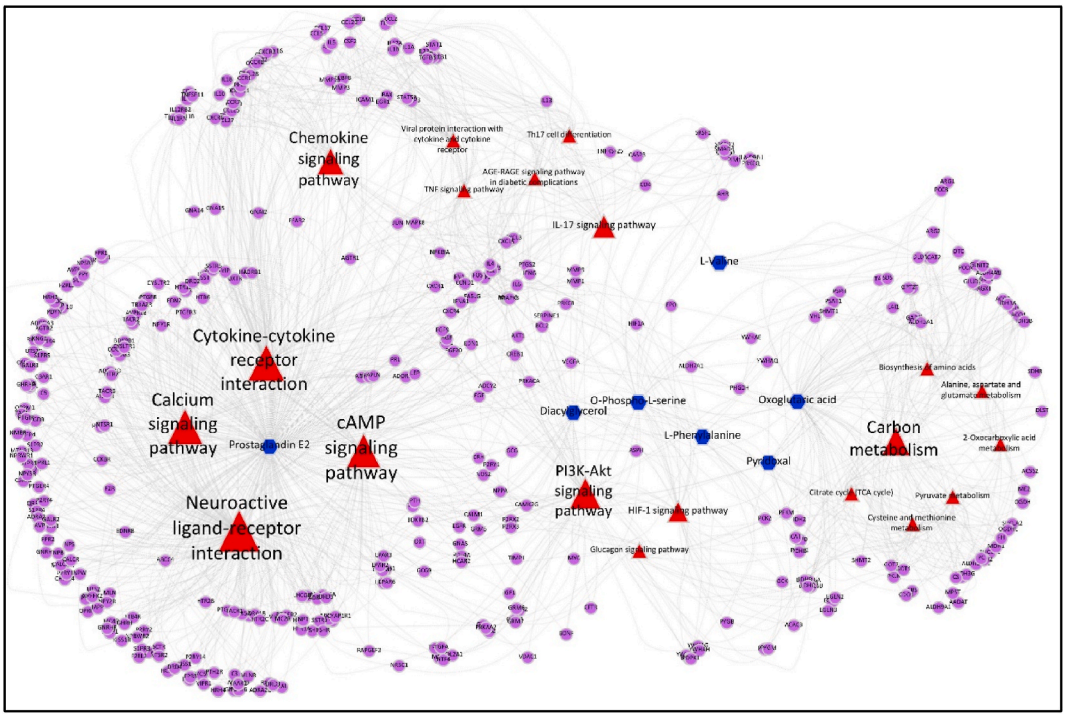

Fig. 9. Relationship network of identified metabolites and DEGs changed by BGZ in KYDS rats. Input metabolites were shown in blue, input genes were shown in purple, related pathways were shown in red, and the triangle size was based on the *P* value.

cAMP and 17-OH-CS in KYDS rats ($P < 0.01$, $P < 0.001$, respectively) (Fig. 10A–B). Although TSH levels did not significantly change in the KYDS group, a marked increase was observed following BGZ treatment (Fig. 10C). Additionally, RT-qPCR analysis revealed that Camkk1, a negative feedback regulator of cAMP, was significantly decreased in KYDS rats treated with BGZ ($P < 0.01$) (Fig. 10D). Similarly, ATP binding cassette subfamily C member 4 (ABCC4), the cAMP efflux transporter, demonstrated a significant reduction in KYDS rats treated with BGZ ($P < 0.05$) (Fig. 10E). Furthermore, BGZ treatment significantly inhibited the expression of protein kinase A (PKA) and promoted the expression of the exchange protein activated by cAMP (EPAC) in KYDS rats ($P < 0.001$ for both) (Fig. 10F–G). The findings further revealed that BGZ significantly inhibited the mRNA expressions of NF-kB, IL-1β, and IL-6 in the downstream target pathway of PKA in KYDS rats ($P < 0.01$, $P < 0.05$, $P < 0.001$, respectively) (Fig. 10H–J). Additionally, BGZ significantly increased the mRNA expression of ERK in KYDS rats, a gene negatively regulated by hydrocortisone ($P < 0.01$) (Fig. 10K). Interestingly, compared to the KYDS group, PI3K and AKT expressions in the KYDS + BGZ group were significantly reduced, with no significant differences observed between the KYDS group and the CON group (Supplemental Fig. 6). The proposed mechanism of BGZ action on the cAMP signaling pathway is depicted in Fig. 10L.

3.11. Molecular docking of active compounds and cAMP signaling pathway-associated proteins

A total of 16 active components of BGZ were collected from the ETCM database for molecular docking analysis. Proteins associated with the cAMP signaling pathway, including EPAC (4MH0), PKA (4Z83), ERK (6G9N), and IL-1β (5R88), were selected as targets for this analysis. As shown in Table 4, at least 13 active compounds demonstrated the ability to access and bind effectively to the active pockets of all proteins associated with the cAMP signaling pathway, exhibiting docking scores below −5 kcal/mol. This suggests that these 13 components within BGZ could be potential contributors to the regulation of the cAMP signaling pathway. Visual representations of the docking interactions between cAMP signaling pathway-associated proteins and a representative BGZ component, bakuchalcone, are presented in Fig. 11.

4. Discussion

KYDS, as described in TCM, is characterized by a cluster of symptoms, including soreness and weakness in the waist and knees, fatigue, general chills, hearing impairment, and tooth loss [25]. Modern pharmacological investigations have indicated that KYDS is primarily associated with disruptions in energy metabolism and imbalances in heat regulation [26]. This study demonstrated a notable improvement in the liver injury condition of KYDS rats following treatment with BGZ. Comprehensive analyses, incorporating both metabolomics and transcriptomics revealed significant alterations in the profiles of endogenous metabolites and DEGs in the livers of KYDS rats treated with BGZ. The integration of metabolomic and transcriptomic data suggests that BGZ may exert hepatoprotective

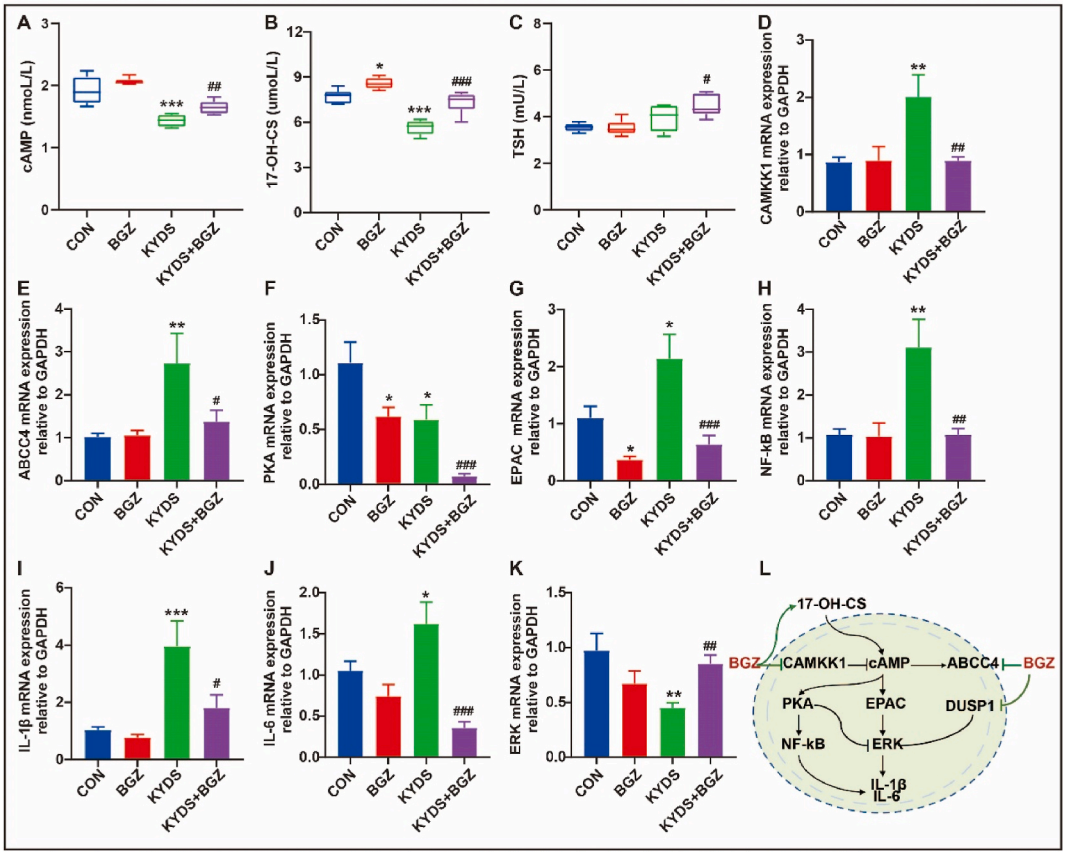

Fig. 10. cAMP signaling pathway alterations in KYDS rats with BGZ treatment (N = 8). The protein expression of cAMP (A), 17-OH-CS (B), and TSH (C) were detected by ELISA. The mRNA expression of *CAMKK1* (D), *ABCC4* (E), *PKA* (F), *EPAC* (G), *NF-kB* (H), *IL-1β* (I), *IL-6* (J), and *ERK* (K) were detected by RT-qPCR. The potential mechanism of BGZ regulating the cAMP signaling pathway in KYDS rats is based on the results (L). $^{*}P < 0.05$, $^{***}P < 0.01$, $^{***}P < 0.001$, compared with CON group; $^{\#}P < 0.05$, $^{\#\#}P < 0.01$, $^{\#\#\#}P < 0.001$, compared with KYDS group.

Table 4
Binding energy (kcal/mol) of the components of BGZ and cAMP signaling pathway-associated proteins.

Compound	Docking scores (kcal/mol)			
	EPAC (4MH0)	PKA (4Z83)	ERK (6G9N)	IL-1β (5R88)
Bakuchalcone	−8.16	−7.67	−8.61	−6.30
Bakuchicin	−7.05	−6.31	−7.42	−5.30
Bakuchiol	−4.09	−3.69	−4.57	−2.09
Bavachalcone	−7.66	−5.93	−8.66	−5.46
Bavachinin	−7.31	−4.20	−7.50	−4.75
Corylidin	−5.81	−5.95	−6.34	−5.97
Corylinal	−4.46	−6.39	−7.84	−5.57
Delphinidin	−5.66	−5.74	−8.25	−5.54
Isobavachalcone	−7.32	−5.81	−7.94	−5.43
Isoneobavachalcone	−8.07	−6.53	−6.35	−5.64
Isopsoralen	−6.83	−7.09	−6.85	−5.28
Neobavachalcone	−8.11	−6.33	−6.27	−5.31
Neobavaisoflavone	−4.98	−7.19	−8.14	−4.46
Psoralen	−7.24	−7.08	−7.06	−5.20
Psoralenol	−6.12	−8.19	−7.38	−5.42
Psoralidin	−5.39	−5.79	−6.71	−5.35

effects by modulating signaling pathways related to energy metabolism in KYDS rats.

Mitochondria, as the central organelles for cellular energy metabolism, apoptosis, immune responses, and signal transduction, play a critical role in maintaining liver function and are particularly vulnerable to drug-induced toxicity [27]. Mitochondrial dysfunction is pivotal in the initiation and progression of various acute and chronic liver diseases [28]. Research indicates that prolonged stress or the

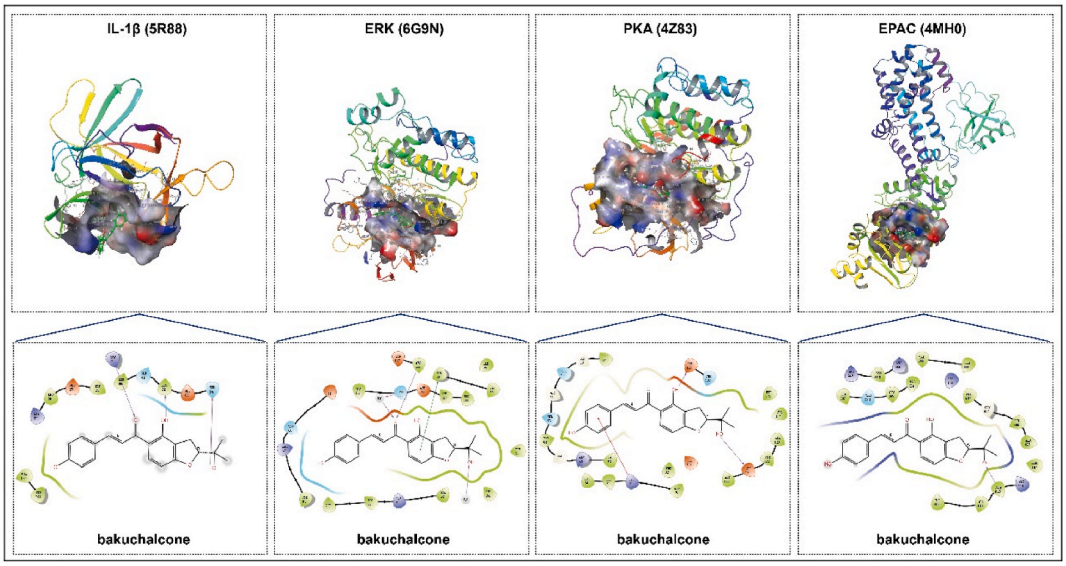

Fig. 11. The molecular docking model (2D and 3D) of representative component (Bakuchalcone) in BGZ and the 4 core targets in the cAMP signaling pathway-associated proteins. In the 2D diagram, the purple arrow indicates the hydrogen bonds and related residues connected, the green line indicates the Pi-Pi stacking bonds and related residues connected, and the red line indicates the Pi-cation stacking bonds and related residues connected.

administration of exogenous hormones, such as hydrocortisone, can induce liver damage by stimulating the generation of reactive oxygen species (ROS) or reactive nitrogen [29]. ROS, acting as an instigator of lipid peroxidation, can enhance the production of malondialdehyde, a byproduct of lipid peroxidation. This process alters the fluidity and permeability of cell membranes, leading to structural and functional changes in cells and ultimately causing oxidative stress-induced injury to liver cells. Glutathione (GSH), the predominant cellular thiol antioxidant, plays a crucial role in countering the oxidative stress triggered by medications, alcohol, dietary factors, and environmental pollutants. Additionally, disruptions in the metabolic equilibrium of GSH have been associated with various liver diseases [30].

GSEA of DEGs revealed that BGZ treatment markedly enhanced OXPHOS and GSH metabolism in KYDS rats. Considering the inclusion of potent antioxidants and modulators of energy metabolism such as psoralen, psoralidin, corylifolin, bakuchiol, and other components in BGZ [31], it is hypothesized that BGZ may confer protection against liver injury induced by KYDS through its antioxidant properties. Furthermore, in this study, we observed a significant elevation in ALDH1B1 expression in KYDS rats, likely linked to lipid peroxidation induced by heightened ROS levels in liver cells [32]. Following intervention with BGZ, the expression of ALDH1B1 appears to be significantly reduced, possibly influenced by the potent inhibitory effects of BGZ and its derivatives on ALDH expression [33]. This further supports the hypothesis that BGZ exerts a protective effect on the liver through its antioxidative properties. The antioxidant efficacy of BGZ has also been substantiated in a study involving dexamethasone-induced muscle atrophy in mice [18].

Mitochondrial dysfunction not only impairs OXPHOS and electron chain transfer but also affects the production of the second messenger cAMP within the mitochondria. KEGG functional analysis of metabolites and DEGs suggests that the cAMP signaling pathway may play a crucial role in the therapeutic effects of BGZ on KYDS rats. cAMP acts as a central second messenger for the transmission of vital life information. It is primarily generated through the binding of G protein-coupled receptors (GPCR) with hormones (such as TSH, ACTH) and neurotransmitter ligands. This process involves the activation of adenylate cyclase (AC), which catalyzes the conversion of adenosine triphosphate (ATP) to cAMP [34,35]. Intramitochondrial cAMP production regulates OXPHOS and ROS generation [36].

The phytohormonal effects of BGZ likely contributed to the significant increase in TSH and 17-OH-CS levels observed in KYDS rats following BGZ administration [37]. Additionally, BGZ demonstrated an inhibitory effect on the expression of Ca/calmodulin-dependent protein kinase 1 (CAMKK1), responsible for regulating cAMP concentration by inhibited ATP catalysis by AC and converting cAMP and phosphorylating cAMP to 5′ AMP [38]. Moreover, ABCC4, a multidrug resistance-associated protein/canalicular multispecific organic anion transporter-related transporter that facilitates the efflux of cAMP from the cytoplasm, was found to reduce intracellular cAMP levels in the colon adenocarcinoma cell line HT29 [39].

In addition, elevated ABCC4 expression and reduced extracellular cAMP levels were observed in KYDS rats, with BGZ treatment reversing this pattern. This suggests that the upregulation of cAMP expression may be attributed, in part, to the inhibition of cAMP efflux. Previous studies have indicated that BGZ can stimulate osteogenic differentiation of bone marrow mesenchymal stem cells (MSCs) through modulation of the cAMP/PKA/CREB signaling pathway [40]. Additionally, other research reported an increase in serum cAMP levels in ovalbumin-sensitized asthmatic rats treated with the total coumarin extract from BGZ [41]. Hence, the elevation of cAMP expression by BGZ in KYDS rats may be attributed to the promotion of hormone expression, inhibition of negative feedback in

the calcium signaling pathway, and the prevention of cAMP efflux or phosphorylation.

cAMP regulates various cellular functions such as lipid metabolism, inflammation, cell differentiation, and injury by modulating gene/protein expression and function [35]. PKA and EPAC serve as direct receptors for cAMP, exerting antagonistic roles in controlling GC sensitivity. PKA and GC collaborate to enhance GC-induced apoptosis, whereas EPAC exhibits a weaker antagonistic effect on GC-induced apoptosis [42]. Augmented intracellular cAMP levels activate both PKA and EPAC.

In this study, BGZ increased cAMP expression while simultaneously reducing the expression of PKA and EPAC, indicating that BGZ has a strong capacity to suppress both PKA and EPAC expression. DUSP1, also recognized as MAP kinase phosphatase-1 (MKP-1), functions as a negative regulator in the MAPK signal transduction pathway. Its expression is induced by GC, leading to increased DUSP1 expression and decreased proteasomal degradation [43]. ERK-1/2, a target of glucocorticoid-mediated negative regulation, requires DUSP1 expression to inhibit ERK-1/2 activation [44,45].

Meanwhile, elevated DUSP1 expression and decreased ERK expression were observed in KYDS rats, while BGZ intervention restored ERK levels to normal. This may be due to the inhibition and stimulation of ERK expression by PKA and EPAC, respectively, which aligns with the observed elevation in EPAC expression and the lack of significant change in PKA in KYDS rats. Therefore, BGZ likely normalizes EKA expression primarily by inhibiting EPAC expression. Molecular docking results indicated that at least 13 components of BGZ, including psoralen and bakuchalcone, may contribute to the therapeutic effects of BGZ on the cAMP signaling pathway. Although the binding energies in this study were not exceptionally strong (docking scores less than −5 kcal/mol), the regulation of cAMP by psoralen and its derivatives supports the hypothesis of BGZ's involvement in cAMP pathway modulation [46,47].

As a downstream target of EPAC, the PI3K/AKT pathway plays a crucial role in promoting cell survival and anti-apoptosis [48]. In many cancer types, activation of the PI3K/AKT pathway enhances the expression of pro-survival proteins such as Bad and caspase-9, thereby fostering resistance to apoptosis in cancer cells [49]. However, the role of the PI3K/AKT pathway in KYDS remains unclear.

In this study, PI3K and AKT expression levels in the liver tissue of KYDS rats did not show significant changes. However, treatment with BGZ led to a reduction in PI3K and AKT levels, suggesting that BGZ may inhibit the activation of the PI3K/AKT pathway in KYDS rats. Transforming growth factor-beta (TGF-beta)-stimulated clone-22 domain family member 1 (TSC22D1), also known as TGFb1i4, is a member of the leucine zipper superfamily. It is highly conserved at both mRNA and protein levels across various species and is known to be highly expressed during the apoptotic phase of early involution [50].

Axin1 up-regulated 1 (AXUD1), also known as cysteine-serine-rich nuclear protein 1 gene (CSRNP1), is a novel nuclear protein that plays a significant role in cell proliferation [51]. Studies have linked the induction of AXUD1 with apoptosis in cementum cells [52], and overexpression of AXUD1 has been found to induce JNK-dependent apoptosis in *Drosophila* [53].

In this study, mRNA expression levels of TSC22D1 and CSRNP1 were significantly elevated in the liver tissue of KYDS rats, indicating that liver cells were in an early apoptotic state. However, BGZ treatment markedly reversed this increase, suggesting that BGZ may help protect liver cells from apoptosis. BGZ has also demonstrated anti-apoptotic effects in other contexts, such as inhibiting renal cell apoptosis in streptozotocin-induced diabetic mice and preventing apoptosis in PC12 cells induced by palmitic acid [54,55]. Conversely, in colorectal cancer cells, prostate cancer PC-3 cells, HepG2 cells, and other tumor cells, BGZ and its monomeric components—such as psoralen, isopsoralen, isobavachalcone, bavachin, and bakuchiol—have been shown to promote apoptosis [56–60].

NF-kB, which is activated by PKA, is a key signaling pathway involved in the expression of inflammatory cytokines, including IL-6 and IL-1β [61]. The liver tissues of KYDS rats exhibited a significant increase in the expressions of IL-6 and IL-1β, indicating the presence of inflammatory infiltration. Following BGZ treatment, the expressions of NF-kB and its downstream inflammatory cytokines IL-6 and IL-1β were significantly reduced. These findings suggest that BGZ may reduce inflammatory infiltration in hepatocytes by suppressing the cAMP/PKA/NF-kB signaling pathway and decreasing the expression of inflammatory cytokines IL-6 and IL-1β.

In conclusion, this study demonstrated that BGZ exerts a protective effect in KYDS rats, primarily by mitigating hepatocyte injury through antioxidative mechanisms, modulation of the cAMP signaling pathway, inhibition of the PKA/NF-kB pathway, and reduction of pro-inflammatory cytokines. Notably, the observed differential effects of high and low doses of BGZ on liver damage and protection are consistent with findings reported in the existing literature. These outcomes are likely attributable to the primary constituents of BGZ, including furanocoumarins, flavonoids, and monoterpenoid phenolic compounds [60,62–64]. This suggests that BGZ may have a dual impact on liver function, underscoring the importance of precise dosage control in clinical applications to ensure effective and safe symptomatic treatment.

However, this study has some limitations. Although the animal model used by the research group closely mimics the behavioral and clinical characteristics of KYDS, including common abnormalities in indicators such as cAMP and cGMP, it does not fully replicate the syndrome's complexity. Developing a more consistent and comprehensive animal model would help to more accurately reflect the therapeutic effects and mechanisms of BGZ, thereby providing a clearer understanding of its potential in clinical applications.

Availability of data and material

We have supplemented the transcriptomic data in the GEO database, and all data can be obtained by the specific website as follows: https://www.ncbi.nlm.nih.gov/geo/query/acc.cgi?acc=GSE249348. We have supplemented the metabolomics data in the MetaboLights database, and all data can be obtained by the specific website as follows: https://www.ebi.ac.uk/metabolights/editor/study/MTBLS10794.

Funding

This work was supported by the National Natural Science Foundation of China (No. 82173993, No. U1904129, No. 82004021), the Key Project of Henan Province for Scientific Research of Traditional Chinese Medicine, China (No. 2019ZYBJ08), and the Key Scientific Research Projects of Colleges and Universities in Henan Province, China (No. 19A360007), and Science and Technology Innovation Team in Universities of Henan Province (No. 23IRTSTHN026).

CRediT authorship contribution statement

Ming-Liang Zhang: Writing – review & editing, Writing – original draft, Visualization, Validation, Supervision, Software, Resources, Project administration, Methodology, Investigation, Formal analysis, Data curation, Conceptualization. **Wei-Xia Li:** Supervision, Software, Resources, Project administration, Methodology, Investigation, Formal analysis, Data curation. **Xiao-Yan Wang:** Supervision, Software, Resources, Project administration, Methodology, Investigation, Formal analysis, Data curation. **Xiao-Fei Chen:** Visualization, Validation, Supervision, Software, Resources, Project administration, Methodology, Investigation, Formal analysis, Data curation. **Hui Zhang:** Visualization, Validation, Supervision, Software, Resources, Project administration, Methodology, Investigation, Formal analysis, Data curation. **Gao-Quan Meng:** Visualization, Validation, Methodology, Data curation. **Yu-Long Chen:** Software, Resources, Project administration, Methodology, Investigation, Formal analysis, Data curation. **Ya-Li Wu:** Software, Resources, Project administration, Methodology, Investigation, Formal analysis, Data curation. **Liu-Qing Yang:** Software, Resources, Project administration, Methodology, Investigation, Formal analysis, Data curation. **Shu-Qi Zhang:** Software, Resources, Project administration, Methodology, Formal analysis, Data curation. **Ke-Ran Feng:** Methodology, Investigation, Formal analysis, Data curation. **Lu Niu:** Software, Resources, Project administration, Methodology, Investigation, Formal analysis, Data curation. **Jin-Fa Tang:** Writing – review & editing, Writing – original draft, Visualization, Validation, Supervision, Software, Resources, Project administration, Methodology, Investigation, Funding acquisition, Formal analysis, Data curation, Conceptualization.

Declaration of competing interest

The authors declare the following financial interests/personal relationships which may be considered as potential competing interests: Jin-Fa Tang reports was provided by National Natural Science Foundation of China. If there are other authors, they declare that they have no known competing financial interests or personal relationships that could have appeared to influence the work reported in this paper.

Appendix A. Supplementary data

Supplementary data to this article can be found online at https://doi.org/10.1016/j.heliyon.2024.e39006.

References]

[1] Z.Y. Shen, Studies of gene networks and singal transduction of kidney deficiency syndrome by syndrome differentiation through drug effects, Zhongguo Zhong Xi Yi Jie He Za Zhi 25 (12) (2005) 1125–1128.
[2] P. Unschuld, Huang Di Nei Jing Su Wen, Nature, Knowledge, Imagery in an Ancient Chinese Medical Text, University of California Press, 2003.
[3] W.B. He, J.L. Zhang, N.H. Chen, Analysis of relationship between brain and kidney of TCM based on negative feedback regulation in hippocampus-HPA axis, China Journal of Traditional Chinese Medicine and Pharmacy 31 (9) (2016) 3426–3428.
[4] V. Scheid, Depression, constraint, and the liver: (Dis)assembling the treatment of emotion-related disorders in Chinese medicine, Cult. Med. Psychiatry 37 (1) (2013) 30–58.
[5] R.B. Lopez, B.T. Denny, C.P. Fagundes, Neural mechanisms of emotion regulation and their role in endocrine and immune functioning: a review with implications for treatment of affective disorders, Neurosci. Biobehav. Rev. 95 (2018) 508–514.
[6] H.P. Xie, et al., Chinese medicine syndrome distribution of chronic hepatitis B virus carriers in immunotolerant phase, Chin. J. Integr. Med. 20 (2) (2014) 94–100.
[7] J. Chen, et al., Serum metabolomics model and its metabolic characteristics in patients with different syndromes of dyslipidemia based on nuclear magnetic resonance, J. Pharm. Biomed. Anal. 167 (2019) 100–113.
[8] Chinese Pharmacopoeia Commission, Pharmacopoeia of the People's Republic of China, Beijing: Chinese Medical, vol. 1, Science and Technology Press, 2020, p. 195.
[9] F. Alam, G.N. Khan, M.H.H.B. Asad, Psoralea corylifolia L: ethnobotanical, biological, and chemical aspects: a review, Phytother Res. 32 (4) (2018) 597–615.
[10] L. Chen, S. Chen, P. Sun, X. Liu, Z. Zhan, J. Wang, Psoralea corylifolia L.: a comprehensive review of its botany, traditional uses, phytochemistry, pharmacology, toxicology, quality control and pharmacokinetics, Chin. Med. 18 (1) (2023) 4.
[11] A.K. Gupta, T.F. Anderson, Psoralen photochemotherapy, J. Am. Acad. Dermatol. 17 (5 Pt 1) (1987) 703–734.
[12] W. McNeely, K.L. Goa, 5-Methoxypsoralen. A review of its effects in psoriasis and vitiligo, Drugs 56 (4) (1998) 667–690.
[13] F.L. Ge, et al., Landscape of hepatobiliary adverse drug reactions related to preparations containing psoraleae Fructus and its application in pharmacovigilance, Chin. J. Integr. Med. 27 (11) (2021) 832–837.
[14] L. Wang, et al., Clinicopathological features of Bu Gu Zhi-induced liver injury, a long-term follow-up cohort study, Liver Int. 40 (3) (2020) 571–580.
[15] R. An, B. Li, L.S. You, X.H. Wang, Improvement of kidney yang syndrome by icariin through regulating hypothalamus-pituitary-adrenal axis, Chin. J. Integr. Med. 21 (10) (2015) 765–771.
[16] S.Y. Chen, et al., Clinical efficacy and transcriptomic analysis of congrong shujing granules ( ) in patients with Parkinson's disease and syndrome of shen (kidney) essence deficiency, Chin. J. Integr. Med. 26 (6) (2020) 412–419.

[17] K. Du, et al., Integrated adrenal and testicular metabolomics revealed the protective effects of Guilingji on the Kidney-Yang deficiency syndrome rats, J. Ethnopharmacol. 255 (2020) 112734.
[18] E. Seo, C.S. Truong, H.S. Jun, Psoralea corylifolia L. seed extract attenuates dexamethasone-induced muscle atrophy in mice by inhibition of oxidative stress and inflammation, J. Ethnopharmacol. 296 (2022) 115490.
[19] Y. Zhang, et al., Comparative studies on chemical contents and effect in kidney-yang deficiency rats of salt-processed product and wine-processed product of cuscutae semen, Evid Based Complement Alternat Med 2019 (2019) 2049497.
[20] D. Kim, B. Langmead, S.L. Salzberg, HISAT: a fast spliced aligner with low memory requirements, Nat. Methods 12 (4) (2015) 357–360.
[21] B. Li, C.N. Dewey, RSEM: accurate transcript quantification from RNA-Seq data with or without a reference genome, BMC Bioinf. 12 (2011) 323.
[22] M.I. Love, W. Huber, S. Anders, Moderated estimation of fold change and dispersion for RNA-seq data with DESeq2, Genome Biol. 15 (12) (2014) 550.
[23] S. Ish-Shalom, A. Lichter, Analysis of fungal gene expression by Real Time quantitative PCR, Methods Mol. Biol. 638 (2010) 103–114.
[24] H.Y. Xu, et al., ETCM: an encyclopaedia of traditional Chinese medicine, Nucleic Acids Res. 47 (D1) (2019) D976–D982.
[25] Z. Shen, The location of deficiency syndrome of kidney Yang, Chin. Med. J. 112 (11) (1999) 973–975.
[26] R.Q. Chen, C.M. Wong, K.J. Cao, T.H. Lam, An evidence-based validation of traditional Chinese medicine syndromes, Compl. Ther. Med. 18 (5) (2010) 199–205.
[27] D.F. Wilson, Oxidative phosphorylation: regulation and role in cellular and tissue metabolism, J. Physiol. 595 (23) (2017) 7023–7038.
[28] A. Mansouri, C.H. Gattolliat, T. Asselah, Mitochondrial dysfunction and signaling in chronic liver diseases, Gastroenterology 155 (3) (2018) 629–647.
[29] A. Vurmaz, E. Atay, Antioxidant effects of piperine on steroid-induced hepatotoxicity, Eur. Rev. Med. Pharmacol. Sci. 25 (17) (2021) 5500–5506.
[30] Y. Chen, H. Dong, D.C. Thompson, H.G. Shertzer, D.W. Nebert, V. Vasiliou, Glutathione defense mechanism in liver injury: insights from animal models, Food Chem. Toxicol. 60 (2013) 38–44.
[31] G. Xiao, et al., Isolation of antioxidants from Psoralea corylifolia fruits using high-speed counter-current chromatography guided by thin layer chromatography-antioxidant autographic assay, J. Chromatogr. A 1217 (34) (2010) 5470–5476.
[32] D. Stagos, et al., Aldehyde dehydrogenase 1B1: molecular cloning and characterization of a novel mitochondrial acetaldehyde-metabolizing enzyme, Drug Metab. Dispos. 38 (10) (2010) 1679–1687.
[33] C.D. Buchman, T.D. Hurley, Inhibition of the aldehyde dehydrogenase 1/2 family by psoralen and coumarin derivatives, J. Med. Chem. 60 (6) (2017) 2439–2455.
[34] D.M.F. Cooper, Compartmentalization of adenylate cyclase and cAMP signalling, Biochem. Soc. Trans. 33 (Pt 6) (2005) 1319–1322.
[35] M. Zaccolo, A. Zerio, M.J. Lobo, Subcellular organization of the cAMP signaling pathway, Pharmacol. Rev. 73 (1) (2021) 278–309.
[36] R. Acin-Perez, E. Salazar, M. Kamenetsky, J. Buck, L.R. Levin, G. Manfredi, Cyclic AMP produced inside mitochondria regulates oxidative phosphorylation, Cell Metabol. 9 (3) (2009) 265–276.
[37] X. Zhang, W. Zhao, Y. Wang, J. Lu, X. Chen, The chemical constituents and bioactivities of Psoralea corylifolia Linn.: a review, Am. J. Chin. Med. 44 (1) (2016) 35–60.
[38] J. Sanchez-Collado, J.J. Lopez, I. Jardin, G.M. Salido, J.A. Rosado, Cross-talk between the adenylyl cyclase/cAMP pathway and Ca2+ homeostasis, Rev. Physiol. Biochem. Pharmacol. 179 (2021) 73–116.
[39] J. Kryczka, E. Sochacka, I. Papiewska-Pająk, J. Boncela, Implications of ABCC4-mediated cAMP eflux for CRC migration, Cancers 12 (12) (2020) 3547.
[40] Y. Han, Y.H. Guo, Y. Yu, Effects of bavachin on regulating differentiation of bone marrow MSC by mediating cAMP/PKA/CREB signaling pathway, Chinese Archives of Traditional Chinses Medicine 37 (7) (2019) 1673–7717.
[41] W.X. Yu, W.Y. Li, H.Y. Li, L. Han, W.L. Chen, S.G. Deng, Effects of total coumarin on cAMP/cGMP of asthmatic rats, Research and Practice of Chinese Medicines (5) (2006) 27–29.
[42] Z. Ji, F.C. Mei, B.H. Johnson, E.B. Thompson, X. Cheng, Protein kinase A, not Epac, suppresses hedgehog activity and regulates glucocorticoid sensitivity in acute lymphoblastic leukemia cells, J. Biol. Chem. 282 (52) (2007) 37370–37377.
[43] O. Kassel, A. Sancono, J. Krätzschmar, B. Kreft, M. Stassen, A.C. Cato, Glucocorticoids inhibit MAP kinase via increased expression and decreased degradation of MKP-1, EMBO J. 20 (24) (2001) 7108–7116.
[44] D.S. Cissel, M.A. Beaven, Disruption of Raf-1/heat shock protein 90 complex and Raf signaling by dexamethasone in mast cells, J. Biol. Chem. 275 (10) (2000) 7066–7070.
[45] L.G. Rider, N. Hirasawa, F. Santini, M.A. Beaven, Activation of the mitogen-activated protein kinase cascade is suppressed by low concentrations of dexamethasone in mast cells, J. Immunol. 157 (6) (1996) 2374–2380.
[46] C.R. Albrightson, R.H. Fertel, B.V. Brown, R. Stephens, Psoralens increase the concentration of cyclic AMP in human cells in vitro, J. Invest. Dermatol. 85 (3) (1985) 264–268.
[47] L. Yin, G. Pang, C. Niu, M. Habasi, J. Dou, H.A. Aisa, A novel psoralen derivative-MPFC enhances melanogenesis via activation of p38 MAPK and PKA signaling pathways in B16 cells, Int. J. Mol. Med. 41 (6) (2018) 3727–3735.
[48] D. Gündüz, C. Troidl, C. Tanislav, S. Rohrbach, C. Hamm, M. Aslam, Role of PI3K/akt and MEK/ERK signalling in cAMP/epac-mediated endothelial barrier stabilisation, Front. Physiol. 10 (2019) 1387.
[49] J.A. Fresno Vara, E. Casado, J. de Castro, P. Cejas, C. Belda-Iniesta, M. González-Barón, PI3K/Akt signalling pathway and cancer, Cancer Treat Rev. 30 (2) (2004) 193–204.
[50] C.A. Huser, et al., TSC-22D1 isoforms have opposing roles in mammary epithelial cell survival, Cell Death Differ. 17 (2) (2010) 304–315.
[51] C.G. Feijóo, A.F. Sarrazin, M.L. Allende, A. Glavic, Cystein-serine-rich nuclear protein 1, Axud1/Csrnp1, is essential for cephalic neural progenitor proliferation and survival in zebrafish, Dev. Dynam. 238 (8) (2009) 2034–2043.
[52] K. Korb, et al., Inhibition of AXUD1 attenuates compression-dependent apoptosis of cementoblasts, Clin. Oral Invest. 20 (9) (2016) 2333–2341.
[53] A. Glavic, C. Molnar, D. Cotoras, J.F. de Celis, Drosophila Axud1 is involved in the control of proliferation and displays pro-apoptotic activity, Mech. Dev. 126 (3–4) (2009) 184–197.
[54] Y. Lee, H.S. Jun, Y.S. Oh, Protective effect of Psoralea corylifolia L. Seed extract against palmitate-induced neuronal apoptosis in PC12 cells, Evid Based Complement Alternat Med 2016 (2016) 5410419.
[55] E. Seo, H. Kang, Y.S. Oh, H.S. Jun, Psoralea corylifolia L. Seed extract attenuates diabetic nephropathy by inhibiting renal fibrosis and apoptosis in streptozotocin-induced diabetic mice, Nutrients 9 (8) (2017) 828.
[56] Y. Li, et al., Isobavachalcone isolated from Psoralea corylifolia inhibits cell proliferation and induces apoptosis via inhibiting the AKT/GSK-3β/β-catenin pathway in colorectal cancer cells, Drug Des. Dev. Ther. 13 (2019) 1449–1460.
[57] C.H. Lin, S. Funayama, S.F. Peng, C.L. Kuo, J.G. Chung, The ethanol extraction of prepared Psoralea corylifolia induces apoptosis and autophagy and alteres genes expression assayed by cDNA microarray in human prostate cancer PC-3 cells, Environ. Toxicol. 33 (7) (2018) 770–788.
[58] Y. Wang, C. Hong, C. Zhou, D. Xu, H.B. Qu, Screening antitumor compounds psoralen and isopsoralen from Psoralea corylifolia L. Seeds, Evid Based Complement Alternat Med 2011 (2011) 363052.
[59] Y. Yang, et al., Bavachin induces apoptosis through mitochondrial regulated ER stress pathway in HepG2 cells, Biol. Pharm. Bull. 41 (2) (2018) 198–207.
[60] Y. Yu, et al., Psoralen induces hepatic toxicity through PERK and ATF6 related ER stress pathways in HepG2 cells, Toxicol. Mech. Methods 30 (1) (2020) 39–47.
[61] S. Gerlo, R. Kooijman, I.M. Beck, K. Kolmus, A. Spooren, G. Haegeman, Cyclic AMP: a selective modulator of NF-κB action, Cell. Mol. Life Sci. 68 (23) (2011) 3823–3841.
[62] N. Qin, et al., Bavachin enhances NLRP3 inflammasome activation induced by ATP or nigericin and causes idiosyncratic hepatotoxicity, Front. Med. 15 (4) (2021) 594–607.
[63] G.Z. Shi, et al., Screening of hepatotoxic compounds in Psoralea corylifolia L., a traditional Chinese herbal and dietary supplement, using high-resolution mass spectrometry and high-content imaging, Biomed. Chromatogr. 35 (9) (2021) e5140.
[64] Y. Wang, et al., Psoralidin, a major component of Psoraleae Fructus, induces inflammasome activation and idiosyncratic liver injury, Int. Immunopharm. 92 (2021) 107352.

Abbreviations

KYDS: Kidney-yang deficiency syndrome
BGZ: Psoraleae Fructus
TCM: traditional Chinese medicine
ALT: alanine aminotransferase
AST: aspartate aminotransferase
ALP: alkaline phosphatase
HE: Hematoxylin and Eosin
cAMP: cyclic adenosine monophosphate
GC: glucocorticoids
ACTH: adreno-cortico-tropic-hormone
CORT: corticosterone
17-OHCS: 17-hydroxycorticosteroids
T3: triiodothyronine
T4: thyroxine
TSH: thyrotropin
cGMP: cyclic guanosine monophosphate
T: testosterone
PCA: principal component analysis
RT: retention time
OPLS-DA: orthogonal partial least-squares discriminant analysis
VIP: variable importance in the projection
KEGG: Kyoto Encyclopedia of Genes and Genomes
GSEA: gene set enrichment analysis
DEGs: differentially expressed genes
OXPHOS: oxidative phosphorylation
ESI+: electrospray positive ion mode
ESI: electrospray negative ion mode
ROS: reactive oxygen species
ALDH1B1: aldehyde dehydrogenase 1 family member B1
ATP: adenosine triphosphate
AC: adenylate cyclase
CAMKK1: Ca/calmodulin-dependent protein kinase 1
ABCC4: ATP binding cassette subfamily C member 4
PKA: protein kinase A
DUSP1: dual specificity phosphatase 1
TSC22D1: transforming growth factor-beta (TGFbeta)-stimulated clone-22 domain family member 1
AXDU1: Axin1 up-regulated 1
CSRNP1: cysteine-serine-rich nuclear protein 1 gene
EPAC: exchange protein activated by cAMP
CYP17A1: Cytochrome P450 family 17 subfamily A member 1
SLC25A25: solute carrier family 25 member 25